Techniques for the Study of Cavitation inside Drops in Microgravity

D. Obreschkow[1,2], P. Kobel[1,3], N. Dorsaz[1,4], A. de Bosset[1], C. Nicollier[5], and M. Farhat[1]
[1] *Laboratoire des Machines Hydrauliques, EPFL, 1007 Lausanne, Switzerland*
[2] *Physics Department, Oxford University, Oxford, OX1 3PU, UK*
[3] *Max Planck Institute for Solar System Research, 37191 Katlenburg-Lindau, Germany*
[4] *Institut Romand de Recherche Numérique en Physique des Matériaux, EPFL, 1015 Lausanne, Switzerland*
[5] *ESA European Astronaut Centre, Cologne, Germany, and NASA Johnson Space Center, Houston, TX*
(Dated: June 2, 2006)

We realized an experimental study of cavitation bubbles inside spherical water drops produced in microgravity (Parabolic Flight Campaigns, European Space Agency ESA). This paper gives a detailed description of the microgravity environment and the experimental techniques.

PACS numbers: 47.55.dp

I. SCIENTIFIC BACKGROUND

The hydrodynamic cavitation phenomenon is a major source of erosion damage in many industrial systems, such as fast ship propellers, cryogenic pumps, pipelines, and turbines. Yet, *controlled* cavitation-erosion proves a powerful tool for modern technologies like ultrasonic cleaning [1], effective salmonella destruction [2], and treatment for kidney stones [3]. Erosive processes are associated with liquid jets and shockwaves emitted by collapsing cavitation bubbles [4], but the relative importance of these two processes remains a topic of debate [5]. Single bubble dynamics strongly depends on nearby surfaces by means of boundary conditions imposed on the surrounding pressure field [6, 7]. Recent investigations revealed interesting characteristics of bubbles collapsing next to flat [8] and curved [30] rigid surfaces or flat free surfaces [11, 34]. It would be fruitful idea to study bubbles inside *spherical drops* and probe their interaction with closed spherical free surfaces. Yet, for larger volumes, such geometries are inaccessible in the presence of gravity and require a microgravity environment, even though gravity plays a negligible *direct* role for most single bubble phenomena.

Stimulated by this situation, we decided to carry out the first experimental study of single bubbles inside centimetric spherical water drops produced in microgravity. The experimental result disclose a wide range of surprising and interesting phenomena, including (1) jet dynamics, (2) shockwave effects and (3) shortened spherical collapse. These results are presented in a physical journal.

II. ZERO-G FLIGHT MANEUVER

The microgravity maneuvers were flown with the Airbus A300 zero-g, a specially equipped aircraft hosted by NOVESPACE at the airport Merignac in France. The nominal flight maneuver is summarized in Fig. 1. From a steady horizontal flight, the aircraft gradually pulls up its nose and climbs to an angle of approximately 47 degrees. This preparatory phase lasts for about 20 seconds, during which the aircraft experiences an acceleration of 1.8 g, oriented perpendicularly to the wing plane. The engine thrust is then suddenly reduced to the minimum required to compensate for air-drag, and the aircraft follows a free-fall ballistic trajectory, i.e. a parabola, lasting for approximately 20 seconds, during which weightlessness is achieved. The residual g-jitter of 0.02-0.05 g at typical frequencies of 1-10 Hz. At the end of this period, the aircraft must pull out of the parabolic arc, a maneuver which gives rise to another 20 second period of 1.8 g. Finally it returns to a steady horizontal flight. These maneuvers are flown repeatedly, 31 times per flight day, with a period of 3 minutes between the start of two consecutive parabolas, i.e. a 1 minute maneuver phase (20 seconds at 1.8 g, 20 seconds below 0.05 g, 20 seconds at 1.8 g), followed by a 2 minute rest phase at 1 g. After parabolas 6, 11, 16, 21 and 26, the rest interval is generally increased to 6 or 8 minutes to allow experimental adjustments.

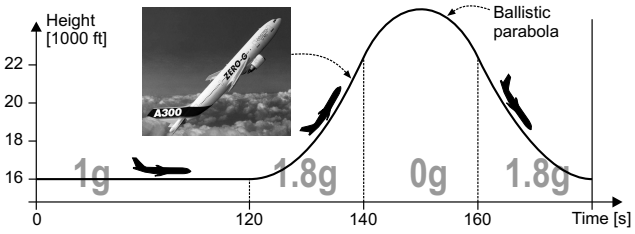

FIG. 1: Nominal Flight Manoeuver with the Airbus A300 zero-g.

III. EXPERIMENT

A. General Setup

Our experiment flew on two different parabolic flight campaigns organized by the European Space Agency ESA (42nd professional parabolic flight campaign, 8th student parabolic flight campaign). Collectively, they sum up to 155 zero-g parabolas on 5 flight days. Each parabola was used to create *one* spherical water drop within 5 s to 15 s and to generate *one* short-lived cavitation bubble inside the drop at the end of its growth. Three physical parameters were independently adjustable: (1) the drop size [radius = 8 mm to

13 mm], (2) the maximal bubble size [radius = 2 mm to 10 mm], (3) the bubble position within the drop [all possibilities].

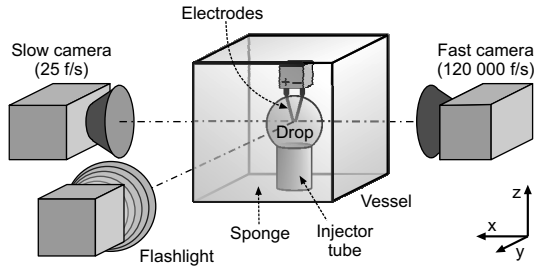

FIG. 2: Configuration of optical system and central components.

Fig. 2 shows the main components of the experimental setup. The studied water drop was contained in a sealed transparent cubic vessel. A standard video camera (Sony Camcorder DCR-TRV900, 25 frames/s) recorded the slow drop growth, whereas a high-speed CCD-camera (Photron Ultima APX, up to 120'000 frames/s) recorded the fast bubble dynamics for a short sequence of 11 ms. This interval was illuminated by a perpendicularly placed high-power flashlight (Cordin Light Source Model 359). A custom-designed computer program triggered the drop creation, bubble generation, image recording and flashlight release. This experimental cycle was initiated automatically at the beginning of each flight parabola, as soon as a stable level of microgravity (< 0.05 g) was achieved. The gravity data was provided by a 100 Hz accelerometer (Memsic, 2125 Dual-axis Accelerometer) that continuously recorded the gravity level during the whole flight.

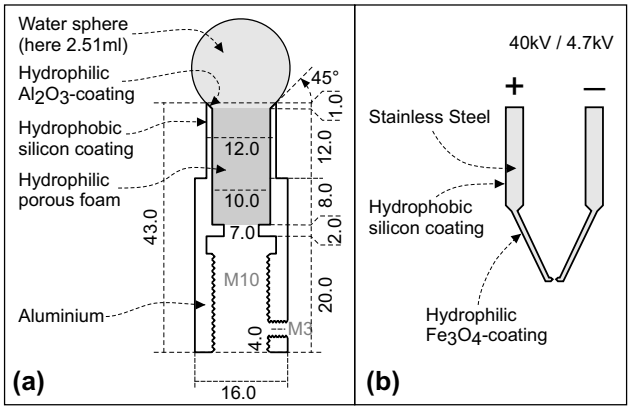

FIG. 3: (a) Detailed measures and coatings of injector tube; lengths in mm. (b) Special coating of electrodes.

The water drop was produced by a computer-controlled micro-pump that smoothly expelled the liquid through a custom-designed injector tube (Fig. 3a). Varying the pumping time allowed to adjust the drop size. In microgravity, the water volume naturally formed a truncated sphere due to surface tension (Fig. 4). This drop remained attached to the injector tube, which permitted to fix the drop's position along the entire parabola and damped out eventual oscillations. After each microgravity phase the water drop fell down and was passively absorbed by sponges covering the vessel bottom.

The cavitation bubble inside the water drop was generated through a fast electrical discharge between two electrodes immersed in the liquid from above (Fig. 4). An initial high voltage (40 kV) formed a plasma allowing the fast discharge of previously charged capacitors (4.7 kV). Shortly after this discharge, the plasma recombined, forming a volume of superheated water vapor that gave rise to a bubble (see [31] for details). In order to minimize the electrodes' interaction with the water volume, their surfaces were specially coated according to Fig. 3b. Using micro stages, the electrodes' position could be varied in the three space dimensions allowing to precisely place the bubble inside the water drop. By stepwisely altering the capacitance between 30 nF and 200 nF, the maximal bubble size could be adjusted according to the relation presented below.

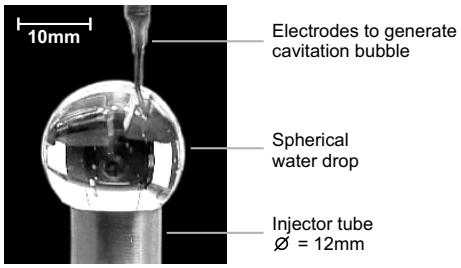

FIG. 4: Quasi-spherical water drop on injector tube in weightlessness. The electrodes penetrate the drop from above.

B. Electrical Discharge Measure

Preliminary ground-based experiments were carried out to determine the fraction of electrical discharge energy transformed in bubble energy. Explicitly, single bubbles were generated inside water volumes, which were very large compared to the bubble size. The maximal bubble radius $R_{b,max}$ was measured for different electrical discharge energies E_e, giving the function $R_{b,max}(E_e)$. The hydrodynamic potential energy E_b at the bubble's maximal size is proportional to its volume by the relation $E_b = \frac{4\pi}{3} R^3_{b,max}(p_\infty - p_V)$, where p_∞ is the water pressure infinitely far from the bubble and p_V the vapor pressure. Hence $R_{b,max}(E_e)$ gives the energy-energy relation $E_b(E_e)$ (Fig. 5). The linear relation reveals that about 32 % of the initial electrical energy was transformed into potential energy of the bubble, whereas 68 % was absorbed elsewhere. The latter fraction was presumably radiated in the *spark shockwave*. Additional sources of energy loss are heat production and light emission.

C. Drop Stability in g-level jitter

In 10% of the zero-g parabolas, we recorded flight-based deviations from the zero-g level larger than 0.05 g for durations longer than 0.2 s. They mostly occurred

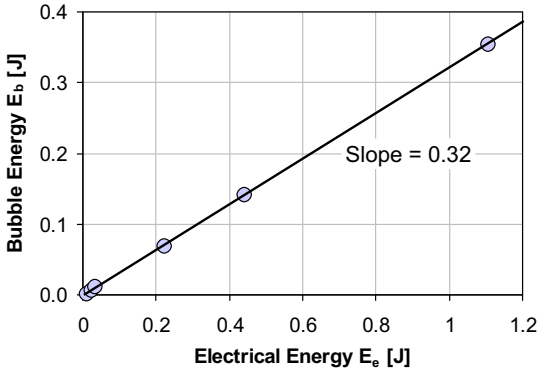

FIG. 5: Bubble energy as a function of electrical energy obtained in preliminary ground-based experiments. (circles) Measured data, (solid line) linear regression.

towards the end of the zero-g cycle, approximately 3 s before the "pull out" command, which terminates the parabola. The injector tube being fixed to the aircraft reference, those fluctuations induced observable oscillations of the water drop, such as shown in Fig. 6. However, such oscillations damp out rapidly within characteristic times of 0.5 s to 1 s. We argue that the large area of support attaching the drop to the tube (1.1 cm^2) is responsible for this efficient attenuation, since the large porous foam ensures an inelastic rebound of the water drop.

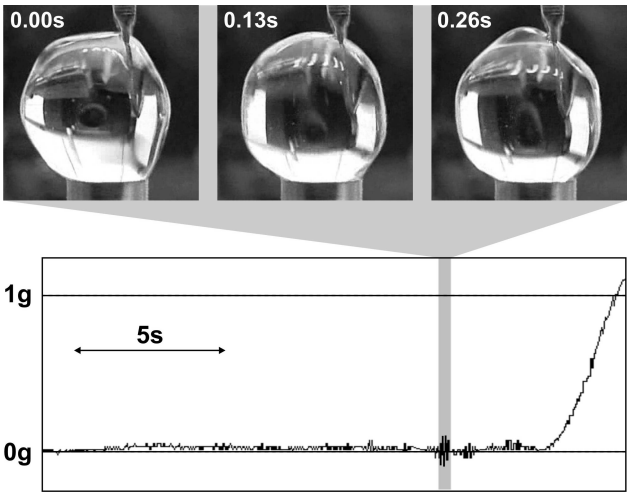

FIG. 6: Water drop oscillations resulting from zero gravity imperfections.

D. Drop Sphericity and Electrodes

Despite of the careful electrode preparation, we observed significant water sphere distortion by electrode-water interaction. During the first flight day, the upper part of the electrodes (thick part) was too hydrophilic yielding oblong distortion of the water volume. Conversely, additional paraffine coverage engendered water repulsion by the electrodes during the initial phase of the second flight day. Digital camera images of ideal spherical, attracted oblong, and repulsed water drops are shown in Fig. 7. Because of this distortion, the electrodes were readjusted during the flight to assure the controlled emission of liquid jets. Moreover, the drops deviations from a perfect sphere render the definition of quantitative parameters such as the curvature ratio between drop and cavity more complex. Hence, comparisons to theoretical models become harder. This reveals the necessity to optimize the electrodes surface coating and to render the tips finer to minimize possible interactions.

FIG. 7: Left: ideal spherical drop (3.5 ml), Center: attracted oblong drop (7 ml), Right: repulsed drop (5 ml).

E. Drop Stability with Cavitation

We observed that the collapsing bubble may induce instabilities on the drop surface or even cause a burst of the entire drop. The physical parameters dictating on the drop's stability are (1) the drop size, expressed by the minimal drop radius $R_{d,min}$ before bubble generation, (2) the bubble size, given by the maximal bubble radius $R_{b,max}$, and (3) the bubble's radial position with in the drop, characterized by the distance d between drop center and bubble center. Only the drop radius $R_{d,min}$ could be read out directly from the images, whereas the other two parameters were subject to optical distortion through refraction at the drop surface. We used a model of optical distortion by a spherical water drop (III F) to reconstitute the true values of $R_{b,max}$ and d from their apparent values. The three parameters $R_{d,min}$, $R_{b,max}$ and d are redundant insofar as a uniform stretching of all parameters reproduces a geometrically similar case. A natural choice of non-redundant parameters is obtained by defining two dimensionless variables: the *relative bubble radius* $\alpha \equiv R_{b,max}/R_{d,min}$ and the *bubble eccentricity* $\varepsilon \equiv d/R_{d,min}$. To study the drop's stability in function of those two quantities, we introduced four stability categories A, B, C, D according to Fig. 8.

Fig. 9 represents the geometries of 35 studied drop-bubble systems in the dimensionless parameter space $\{\epsilon, \alpha\}$. Each point was assigned a stability category allowing to recognize four roughly defined stability domains. Some points appear to lie in the wrong domain, which is explained by the difficulty of distinguishing neighboring stability categories in certain cases. This representation reveals that relative bubble radii above $\alpha_{crit} = 0.53$ lead to a burst of the entire water drop (cat D). A close look at the three samples belonging to this category showed that the drop remains essentially stable during bubble growth and collapse, but explodes

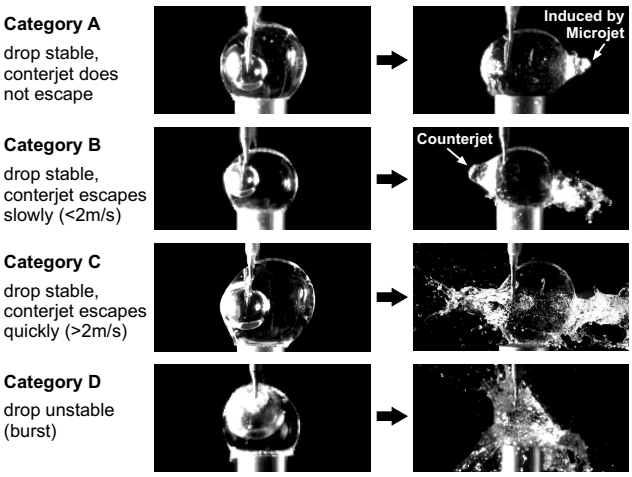

FIG. 8: Four categories, introduced to classify the stability of the water drop and its surface with respect to the bubble implosion. (left images) Maximum bubble size. (right images) Situation 4 ms later.

when the liquid jets disrupt the surface. We also see that eccentricities below 0.3 yield no significant counterjet, although the microjet may still be sufficiently violent to cause an escaping liquid jet (cat A). Finally, we note that for equal relative bubble radii, the counterjet velocity increases with increasing eccentricities ϵ, because of a stronger pressure peak between bubble and free surface [34].

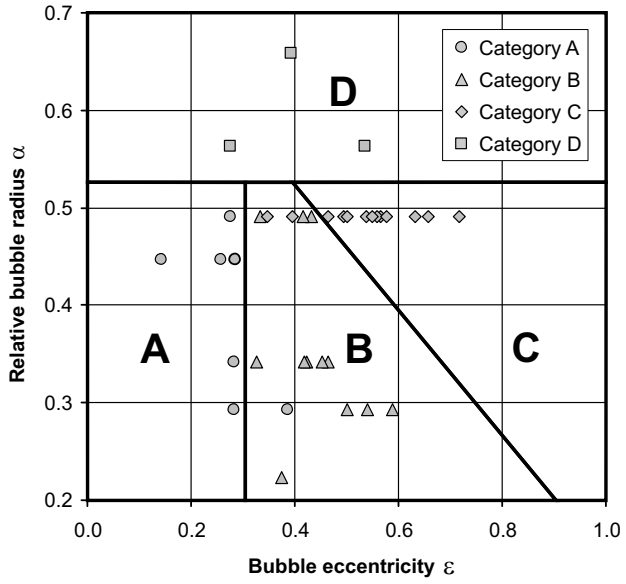

FIG. 9: Four stability-domains in the parameter space {bubble eccentricity ϵ, relative bubble radius α}, according to the four stability classes of Fig 8.

F. Optical Distortion by a Liquid Drop

The image of the bubble inside the water drop is distorted due to optical refraction at the drop's surface. We show that the apparent image is mostly too large, the linear stretching being approximately equal to the index of refraction η_{water}.

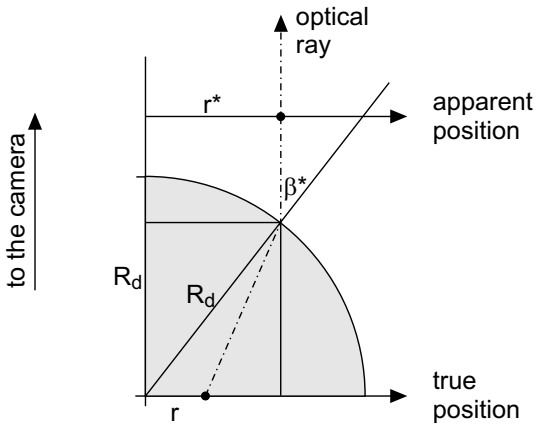

FIG. 10: Model of optical refraction by a spherical drop. (gray zone) Quarter of the drop's cross-section, (dashed line) optical ray.

We consider a point located inside a spherical water drop at a distance r from the drop center and placed perpendicularly to the optical axis (Fig. 10). From outside the drop, the point seems to lie at an *apparent position* r^*. The geometrical problem may be reduced by considering the two-dimensional drop section, which is parallel to the optical axis and contains both the drop center and the observed point. For simplicity only the relevant quarter of the drop section is shown here. From Fig. 10 we derive the geometrical relation

$$r^* - r = \sqrt{R_d^2 - r^{*2}}\ tan(\alpha) = \sqrt{R_d^2 - r^{*2}}\ tan(\beta^* - \beta)$$

where $sin(\beta^*) = r^*/R_d$. To eliminate β, Snell's law of refraction is applied,

$$sin(\beta) = \frac{1}{\eta_{water}} sin(\beta^*) = \frac{r^*}{\eta_{water} R_d}$$

After substitution and rearrangement, the following relation between r and r^* is obtained,

$$r = r^* - \sqrt{R_d^2 - r^{*2}} \cdot tan\left(arcsin\frac{r^*}{R_d} - arcsin\frac{r^*}{\eta_{water} R_d}\right)$$

Fig. 11 (solid line) shows r/R_d in function of r^*/R_d for the particular index $\eta_{water} = 1.33$. Over the wide range $r^*/R_d < 0.6$ this function is nearly linear obeying the simple law (dashed line),

$$r^* = \eta_{water} r \qquad \text{(linear expansion about } r = r^* = 0)$$

IV. ACKNOWLEDGEMENTS

We gratefully acknowledge the *European Space Agency (ESA)* for having offered the possibility to pursue these experiments on parabolic flights. Furthermore, our gratitude is directed to the *Swiss National Science Foundation (SNSF)* who provided the substantial basis of the whole research frame. We also thank

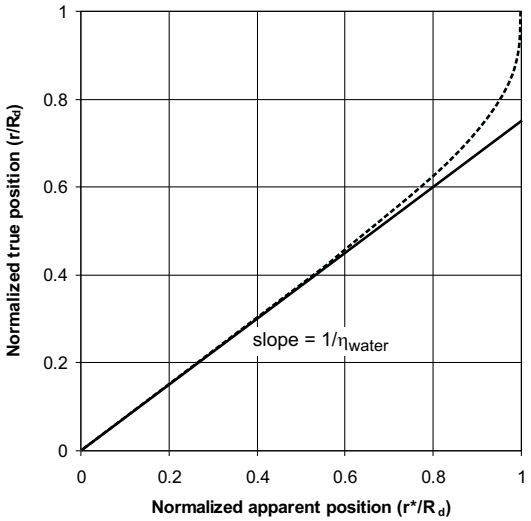

FIG. 11: (solid line) True position versus apparent position of a point inside a water sphere, observed perpendicularly to the straight line connecting it to the spheres center. (dashed line) Linear expansion about $r = r^* = 0$.

several institutions of the *École Polytechnique Fédérale de Lausanne (EPFL)* for their support in financial, practical and theoretical aspects. Finally, we thank our private donator, the *Swiss Space Industry Group (SSIG)*.

[1] W. D. Song, M. H. Hong, B. Lukyanchuk, and T. C. Chong, J. Appl. Phys. **95**, 2952 (2004).
[2] D.M. Wrigley and N. G. Llorca, J. Food Prot. **55**, 678 (1992).
[3] Y.A. Pishchalnikov, O. A. Sapozhnikov, M. R. Bailey, J. C. Williams Jr, R. O. Cleveland, T. Colonius, L. A. Crum, A. P. Evan, J. A. McAteer, J. Endourol. **17**, 435 (2003).
[4] J.-C. Isselin, A. P. Alloncle, and M. Autric, J. Appl. Phys. **84**, 5766 (1998).
[5] A. Shima, shockwaves, **7**, 33 (1997).
[6] M. S. Plesset and R. B. Chapman, J. Fluid Mech. **47**, 283 (1971).
[7] C. E. Brennen, *Cavitation and Bubble Dynamics* (Oxford University Press, 1995).
[8] E. A. Brujan, G. S. Keen, A. Vogel, and J. R. Blake, Phys. Fluids **14**, 85 (2002).
[30] Y. Tomita, R. B. Robinson, R. P. Tong, and J. R. Blake, J. Fluid Mech. **466** 259 (2002).
[34] R. B. Robinson, J. R. Blake, T. Kodama, A. Shima, and Y. Tomita, J. Appl. Phys. **89**, 8225 (2001).
[11] A. Pearson, E. Cox, J. R. Blake and S. R. Otto, Eng. Anal. Bound. Elem. 28, 295 (2004).
[31] F. Pereira, M. Farhat, and F. Avellan, in *Bubble Dyn. and Interface Phen.* (J.R. Blake et al. eds., 227, 1994).
[33] L. A. Crum, J. Phys. **40**, 285 (1979).
[25] E. Robert, MS Thesis, Ecole Polytechnique Federale de Lausanne, Code: LMHDI04R (2004).
[15] L. Rayleigh, Philos. Mag. **34**, 94 (1917).
[16] M. S. Plesset, J. of Appl. Mech. **16** (1949).
[17] T. Kodama and Y. Tomita, Appl. Phys. B, **70**, 139 (2000).
[18] B. Wolfrum, T. Kurz, R. Mettin, and W. Lauterborn, Phys. Fluids, **15**, 2916 (2003).
[19] G. N. Sankin, W. N. Simmons, S. L. Zhu and P. Zhong, Phys. Rev. Lett. **95**, 034501 (2005).
[20] Y. Tomita, T. Kodama, and A. Shima. Appl. Phys. Lett. **59** 274-276 (1991).
[21] www.spaceflight.esa.int/users/index.htm
[22] www.flashandsplash.ch
[23] Avellan F. "Cavitation in Hydraulic Turbines" Keynote Lecture, 5th International Symposium on Cavitation CAV2003, Osaka, Japan. 2003.
[24] Frost D, Sturtevant B. Journal of Heat Transfer-Transactions of the ASME 108 (2): 418-424. May 1986.
[25] Robert E, Master Thesis EPFL LMH. 2004.
[26] Escaler X, Dupont P, Avellan F. "Experimental investigation on forces due to vortex cavitation collapse for different materials." Wear 233(12): 65-74. 1999.
[27] Guennoun F, Farhat M, Ait Bouziad Y, Avellan F, Pereira F. "Experimental Investigation of a Particular Traveling Bubble Cavitation ". Proceedings of the 5th International Symposium on Cavitation CAV2003, Osaka, Japan. 2003.
[28] Lettry J, Fabich A, Gilardoni S, Benedikt M, Farhat M, Robert E. "Thermal shocks and magnetohydrodynamics in high power mercury jet targets". Journal of Physics G: Nuclear and Particle Physics 29(8): 1621-1627. 2003.
[29] Gibson DC, Blake JR. Applied Scientific Research 38: 215-224. 1982.
[30] Tomita Y, Robinson PB, Tong RP, Blake JR. Journal of Fluid Mechanics 466: 259-283. Sept 2002.
[31] Pereira F, Farhat M, Avellan F. "Dynamic calibration of transient sensors by spark generated cavity" in "Bubble Dynamics and Interface Phenomena", 227-240. J.R. Blake et al. (eds.). 1994.
[32] Benjamin TB, Ellis AT. Philosophical Transactions of the Royal Society of London. Series A-Mathematical and Physical Sciences 260 (1110): 221-&. 1966.
[33] Crum LA, Journal de Physique 41: 285-288 Suppl. 8, 1979.
[34] Robinson PB, Blake JR, Kodama T, Shima A, Tomita Y. Journal of Applied Physics 89 (12): 8225-8237. Jun 2001.